International Environmental Modelling and Software Society (iEMSs)
2010 International Congress on Environmental Modelling and Software
Modelling for Environment's Sake, Fifth Biennial Meeting, Ottawa, Canada
David A. Swayne, Wanhong Yang, A. A. Voinov, A. Rizzoli, T. Filatova (Eds.)
http://www.iemss.org/iemss2010/index.php?n=Main.Proceedings

Numerical simulation of transition layer at a fluid-porous interface

Carlo Gualtieri
Hydraulic, Geotechnical and Environmental Engineering Department (DIGA), University of Napoli "Federico II". Italy.
carlo.gualtieri@unina.it

Abstract: The study of flow phenomena at the sediment-water interface is very important in the field of environmental hydraulics. When a porous layer is overlaid by viscous fluid flow, a thin transition zone between the layers is formed, which is responsible for the interfacial momentum and mass transfer. This layer, also referred as Brinkman layer, is associated with the depth of penetration of the influence from the free-fluid region.
This paper presents the preliminary results of numerical simulation of the flow in a rectangular geometry representing the region around the interface between a fluid and a porous media. The geometry reproduces that experimentally investigated by Goharzadeh et al. [2005]. The flow was described by the Navier-Stokes equations in the free region and the Brinkman equation in the porous region. Numerical simulations were carried out in laminar steady-state flow using Multiphysics 3.5a, a CFD code, in a range of Darcy number *Da* from 8.13×10^{-8} to 2.43×10^{-6} and of fluid-based Reynolds number Re_f from 6 to 21. The thickness of the transition layer, defined as the height below the permeable interface up to which the velocity decreases to Darcy scale was measured from the simulated flow field. Numerical data were generally lower than the experimental data, but they were in agreement with the observed trends because the thickness of the transition layer increased with the increasing *Da* whereas it was not greatly altered by the increasing Re_f.

Keywords: Environmental hydraulics, fluid-porous interface, transition layer, CFD, Brinkman equations, experimental validation

1. INTRODUCTION.

Flow phenomena and the associated mass and momentum transfer near a porous medium/free flow interface are of great theoretical and practical interest. They are found in various fields, such as environmental hydraulics, geophysical fluid dynamics, and mechanical engineering among others. In the area of environmental hydraulics, the main problem is on clarifying how the free flow in a natural channel will interact with the porous bed, and how the mass, dissolved organic molecules, inorganic ions and fluid/gas flux, and momentum will transfer across the free flow/porous bed interface since it may greatly affect water quality in both the channel and the bed. For example, the exchange of solutes between the sediment and the water is strongly related to the near-bed shear velocity (Steinberger and Hondzo, [1999]; Higashino et al., [2003]; Gualtieri, [2004]; Gualtieri, [2005]; Higashino and Stefan [2008]) and near-bed turbulence reduces the mean hitting time of fine organic particles, resulting in a continuous redistribution of organic particles, which increases the availability of resources near the bed (McNair et al., [1997]). The near-bed turbulence also affects the benthic ecology because it controls mass transfer processes on permeable river beds (Huettel et al., [2003]; Lorke et al., [2003]; Packman et al., [2004]).
Flows over a porous medium are characterized by a hybrid clear fluid-porous medium domain that flows both over and through the porous medium. The internal flow field of the porous medium remains coupled with the overlying fluid. The complex interaction between the overlying fluid and the internal fluid means the no-slip surface boundary condition is no longer applicable (James and Davis, [2001]; Chan et al., [2007]). Thus, the fluid/porous interface problem, the flow interaction above and inside the porous medium, and the transfer mechanisms across the interface, deserve in-depth investigation. This paper

presents some results of numerical simulation of the flow in a 2D geometry representing the region around the interface fluid-porous interface. The geometry reproduces that experimentally investigated by Goharzadeh et al. [2005]. The flow was described by the Navier-Stokes equation in the free region and the Brinkman equations in the porous region. Numerical simulations were carried out in laminar steady-state flow using Multiphysics 3.5a in a range of Darcy number *Da* from 8.13×10^{-8} to 2.43×10^{-6} and of fluid-based Reynolds number Re_f from 6 to 20.99 to point out the influence of these parameters on the flow field characteristics. Also, the influence of the fluid height on the flow field was evaluated. The thickness of the transition layer, defined as the height below the permeable interface up to which the velocity decreases to Darcy scale, was finally obtained from the numerical velocity outputs and compared with the experimental findings of Goharzadeh et al. [2005].

2. FLOW PROCESSES AT THE SEDIMENT-WATER INTERFACE.

The flow of viscous fluids in a channel can be described by Navier-Stokes equations. Inside a porous medium, the global transport of momentum by shear stresses in the fluid is often negligible because the pore walls impede momentum transport to the fluid outside the individual pores. Also, although at the fundamental *microscopic* level these equations still apply, it is quite difficult to obtain their solution considering the complexity and often only statistically known geometry of the solid surfaces in the medium. Hence, a homogenization of the porous and fluid media into a single medium is a common alternative approach and the flow in a porous medium is usually described by volume averaged equations, such as the empirical Darcy's law, which states that the volume averaged velocity field is determined by the pressure gradient, the fluid viscosity and the structure of the porous medium:

$$\langle \vec{V} \rangle = -\frac{k}{\mu} \nabla \langle p \rangle \qquad (1)$$

where μ is fluid dynamic viscosity [$M\cdot L^{-1}\cdot T^{-1}$], k is porous medium permeability [L^2], which is a scalar for an isotropic porous medium, and p is the pressure [$M\cdot L^{-1}\cdot T^{-2}$]. These averaged or *macroscopic* properties are defined at any point inside the medium by means of averaging of the actual fluid properties over a certain volume surrounding the point. The volume is small compared to the typical macroscopic dimensions of the problem, but it is large enough to contain many pores and solid matrix elements. Eq. 1 together with the continuity equation and equation of state for the pore fluid provide a complete mathematical model suitable for a wide variety of applications involving porous media flows, where the pressure gradient is the major driving force.

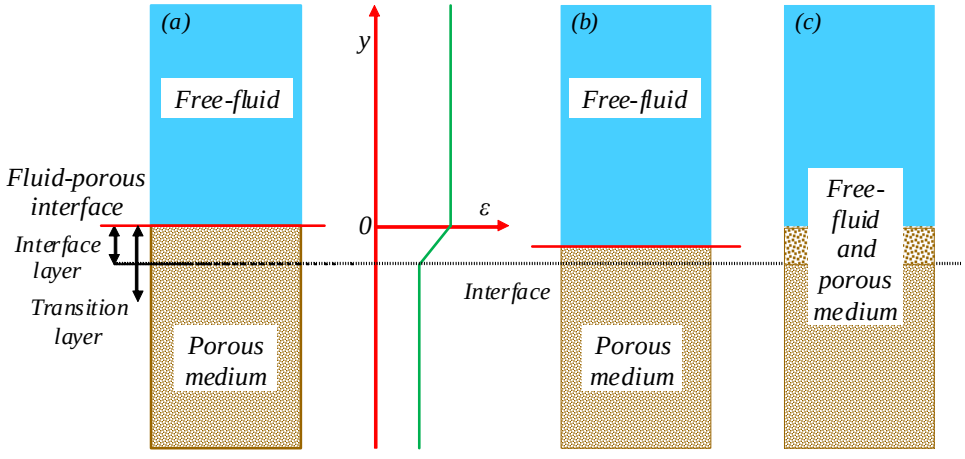

Figure 1. Macroscopic flow above and within a porous medium.

If the porous medium is bounding an open channel flow two intuitively clearly distinct flow regions exist and the *no-slip* condition at the surface of the porous medium generally does not apply (Fig.1). The *free-fluid* region above the permeable wall, where there is no solid matrix so porosity is one, and the *porous medium* region, where porosity is less than one

(Fig.1a) (Pokrajac and Manes, [2008]). Note that porosity ε is defined as the fraction of the control volume within the porous medium, which is occupied by pores. In the free-fluid region flow features resemble those of boundary layer flows, whereas below the fluid-porous interface the flow has the features of porous media flows. Across the fluid-porous interface there is the need to establish continuity of fluid velocities and stresses. Two possibilities hold. The transition between the flow above and inside the permeable wall may be *sharp* (Fig.1b), so the flow variables may have a step change across the macroscopic boundary. Alternatively, if there is a sufficient degree of continuity, flow variables gradually change between the two regions and the transition is *smooth* (Fig.1c). In the literature, sharp transition is associated with the two-domain simulation models and the smooth transition with the single-domain models, as below described.

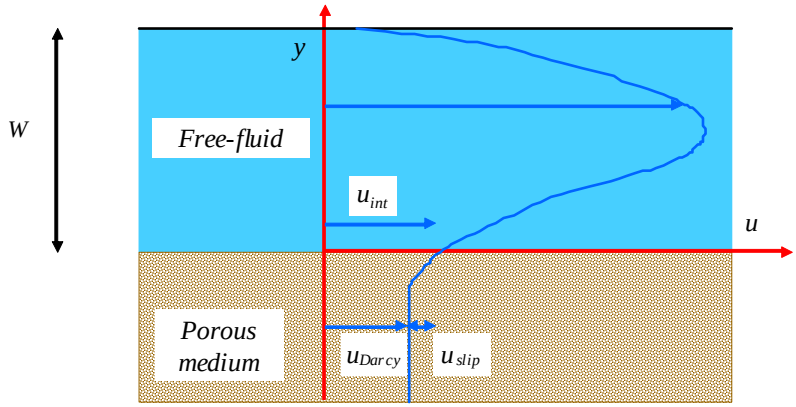

Figure 2. Velocity profile for pressure-driven planar flow in a channel/porous medium.

Since there is effectively a slip velocity at the surface, previous studies of interfacial flow have focused on the dependence of this velocity on the characteristics of the medium and the external flow. Consider a laminar flow in the channel which is driven by pressure, where W is channel width (Fig.2). The velocity profile away from the interface is parabolic and approaching the fluid-porous interface the velocity is decreasing down to u_{int}, which is the velocity at the interface. Herein, the higher free-fluid momentum is transferred into the pores via viscous stress. Below the interface, inside the porous medium, there is a layer where the flow is influenced by the free-flow field and the velocity of fluid particles decreases drastically, until it reaches an averaged constant velocity which is predicted by Darcy equation u_{Darcy}. This layer is usually termed *transition layer* or *Brinkman layer* (Fig.1c). This thin layer is responsible for the interfacial momentum and mass transfer and it acts as transition layer between the realms of the Navier-Stokes equations and the Darcy equation (Goharzadeh et al., [2005]). Besides the transition layer, a space necessary for the solid matrix to achieve the geometrical properties of the porous medium must be considered (Fig.1b), namely ε (Pokrajac and Manes, [2008]). This is termed *interface layer*, which is hence defined by the geometry of the pore space while the transition layer is related to flow conditions. Thus, these two layers have clearly defined and different physical properties.

The above discussion pointed out that there are two general approaches to describe macroscopic flow within the transition layer, both developed for laminar boundary layer flows: sharp interface and smooth interface approach (Pokrajac and Manes, [2008]).

The first approach consists of two homogeneous regions divided by a sharp interface, which is selected somewhere within the interface region (Fig.1b). At this interface an appropriate conditions, usually expressed as a step change in some spatially averaged flow variable, is adopted. Beaver and Joseph [1967] introduced a slip velocity u_{slip}, which was defined as the difference between the free-flow velocity at the interface u_{int} and the Darcian velocity u_{Darcy} far away from the interface, below the transition layer (Fig.2). They proposed that, for the for the planar geometry shown in Fig. 2, the slip velocity is proportional to the velocity gradient in the open channel at the interface:

$$U_{slip} = \frac{k^{1/2}}{\alpha} \left. \frac{du}{dy} \right|_{y=0^+} \qquad (2)$$

where α is a dimensionless slip coefficient, which was assumed to be the property of the porous medium architecture and independent of the fluid viscosity. Several researchers investigated the slip coefficient α, pointing out that it is very sensitive to the adopted location of the interface (James and Davis, [2001]; Pokrajac and Manes, [2008]). Other authors assumed continuity of the velocity at the fluid-porous interface and proposed different shear stress condition (Vafai and Kim, [1990]; Ochoa-Tapia and Whitaker, [1995]).
The second approach assumes a continuous transition between the free-fluid and the homogeneous porous medium (Fig.1c). The physical properties of the fluid are defined as intrinsic volume averages that corresponds to a unit volume of pores and are assumed to be continuous over the interface region. The flow velocities are defined as superficial volume averages and they correspond to a unit volume of the medium including both pores and matrix. Thus, the velocity field is continuous across the fluid-porous interface. This approach eliminates the need for explicit consideration of interfaces and the flow can be modeled by using the same variables for the entire domain, but flow equations need to be properly adjusted to reflect the change of physics above introduced. This approach was first proposed by Brinkman [1947], who added a macroscopic viscous shear stress term, with fluid viscosity, to Eq. (1), in order to account for the velocity gradient in the transition layer:

$$-\nabla\langle p\rangle-\frac{\mu}{k}\langle\vec{V}\rangle+\mu'\nabla^2\langle\vec{V}\rangle=0 \qquad (3)$$

where μ' is the *apparent* or *effective* viscosity. Several theoretical and numerical studies were proposed to quantify the dependency of μ' from both porous medium characteristics and fluid viscosity (Tan and Pillai, [2009]). Often $\mu'=\mu$ for simplicity, but, if porosity is high, this assumption leads to an overestimation of the interfacial velocity and to high flowrate through the free-fluid domain. Comparing Eq. (1) and Eq. (3), if the pressure gradient is applied in the *x*-direction only and the superficial velocity gradients exist in the y-direction only, the last term in Eq. (3) may be considered as interpolating the interfacial velocity u_{int} and the Darcian velocity u_{Darcy} and this decay is (Gupte and Advani, [1997]):

$$u=u_{Darcy}+\left(u_{int}-u_{Darcy}\right)exp\left[\frac{y}{k^{1/2}\left(\mu'/\mu\right)^{1/2}}\right] \qquad (4)$$

This is a solution of Eq. (3) which meets the following boundary conditions:

$$\begin{aligned} u&=u_{Darcy} \quad \text{as} \quad y\to\infty \\ u&=u_{int} \quad \text{as} \quad y=0 \end{aligned} \qquad (5)$$

Interestingly, Eq. (1) and Eq. (3) yield an identical value of u_{int} if the slip coefficient α introduced in Eq. (1) is assumed to be equal to $(\mu'/\mu)^{1/2}$, that is the square root of the ratio between the effective viscosity and the fluid viscosity (Gupte and Advani, [1997]).
Original Brinkman equation was modified by Ochoa-Tapia and Whitaler [1995] as:

$$-\nabla\langle p\rangle-\frac{\mu}{k}\langle\vec{V}\rangle+\frac{\mu}{\varepsilon}\nabla^2\langle\vec{V}\rangle=0 \qquad (6)$$

which is identical to Eq. (1) except $\mu'=\mu/\varepsilon$ and is termed *modified* Brinkman equation. Several studies were carried out assuming a variable permeability and a combination of variable permeability and viscosity (Pokrajac and Manes, [2008]). The approach based on Brinkman equation has the advantage to predict a transition layer thickness which is on the order of $k^{1/2}$, as suggested in many theoretical studies, but the variable parameters that give accurate prediction of the velocity profiles cannot be given in a general form.

3. NUMERICAL MODELLING OF FLOW PROCESSES AT THE FLUID-POROUS INTERFACE.

As above explained, the smooth or single-domain approach allows to consider the same unknown variables for the entire domain including both free-flow and porous medium regions. The distinction is made by switching on and off certain terms in the governing equations. This approach was applied in this numerical study. Free-fluid flow was simulated

by using the well-known mass conservation and momentum balance equations. For a planar, steady-state and incompressible flow, they are:

$$\frac{\partial u}{\partial x}+\frac{\partial v}{\partial y}=0 \tag{7}$$

$$\rho\left(u\frac{\partial u}{\partial x}+v\frac{\partial u}{\partial y}\right)=-\frac{\partial p}{\partial x}+\mu\nabla^2 u+F_x$$
$$\rho\left(u\frac{\partial v}{\partial x}+v\frac{\partial v}{\partial y}\right)=-\frac{\partial p}{\partial y}+\mu\nabla^2 v+F_y \tag{8}$$

where in the Navier-Stokes equations, ρ is fluid density, p is fluid pressure, F_x and F_y are force terms accounting for gravity or other body forces, and u, v are velocity components in the x and y directions, respectively.
In the porous medium, the governing equations are again continuity and momentum balance equations. For a planar, steady-state and incompressible flow, continuity equation is Eq. (7), while momentum balance equations in a porous medium are:

$$\frac{\mu}{k}u=-\frac{\partial p}{\partial x}+\frac{\mu}{\varepsilon}\nabla^2 u+F_x$$
$$\frac{\mu}{k}v=-\frac{\partial p}{\partial y}+\frac{\mu}{\varepsilon}\nabla^2 v+F_y \tag{9}$$

Note that Eq. (9), which is formally identical to Eq. (6), can be obtained from Eq. (8) replacing in the left-hand side the advective term by the Darcian term and assuming the porosity different from 1.

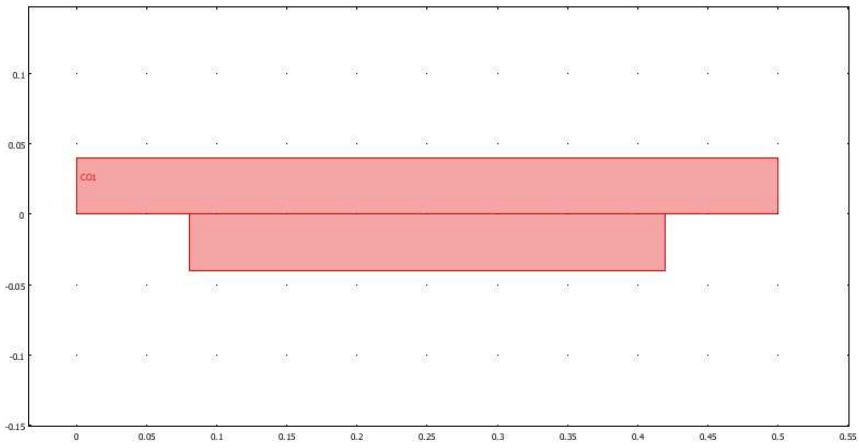

Figure 3. The investigated geometry.

These equations were solved using Multiphysics 3.5a™ modeling package, which is a commercial multiphysics modeling environment (Multiphysics, [2008]). It solved Eqs. from (7) to (9) for the pressure p and the velocity vector components u and v within the entire domain of the flow. Multiphysics 3.5a™ was applied to the geometry presented in Fig.3, which is the lateral view of the channel used by Goharzadeh et al. in their experimental works in laminar flow over a porous medium (Goharzadeh et al., [2005]). They conducted their experiments in a rectangular flume 0.50 m long, 0.10 m wide and 0.05 m high. The central region of the extent 0.34×0.04×0.05 m was filled by a random packing of a porous sample. Experiments were conducted using five different types of transparent borosilicate monodisperse glass beads and polydisperse granulates with physical properties listed in Table 1, where d is the grain size. The porosity and permeability were measured separately by laboratory experiments. The porous material was embedded between two 0.05×0.05 m filters. The upper surface of the porous bed was flattened with a solid object to ensure a horizontal interface. The flume was then filled with a silicon oils mixture with density ρ=1006 Kg/m³, dynamic viscosity μ=4.28×10^{-2} Kg/m×s and kinematic viscosity ν=42.5×10^{-}

^{6} m²/s. The height of the porous layer was constant for all experiments h_p=0.04 m. A uniform pressure gradient was maintained in the longitudinal direction of the channel by a pump with an approximate maximal flow capacity of Q=5 L/min (Goharzadeh et al., [2005]). Using particle image velocimetry (PIV) and refractive index matching (RIM), two-dimensional velocity measurements in the interfacial region were performed. The thickness of the Brinkman or transition layer δ_{Brink} was evaluated from the experimental data using two approaches. The first criterion was based on a statistical test and the second one assumed boundary layer thickness definitions, as below explained in details (Goharzadeh et al., [2005]).

Table 1. Physical properties of the porous medium: glass beads (GB) and granulates (GL)

Samples	d - cm	k - m²	ε
GL1	0.05–0.2	$5.2\times10^{-10}\pm8.8\times10^{-12}$	0.43±0.01
GL2	0.2–0.35	$3.9\times10^{-9}\pm6.7\times10^{-11}$	0.41±0.01
GB1	0.25	$5.2\times10^{-9}\pm8.4\times10^{-11}$	0.38±0.01
GB2	0.47	$1.1\times10^{-8}\pm3.1\times10^{-10}$	0.41±0.01
GB3	0.65	$1.3\times10^{-8}\pm6.9\times10^{-10}$	0.41±0.01

In the experiments, flow conditions were characterized by using a number of different Reynolds numbers. First, a classical fluid-based Reynolds number was defined as

$$Re_f = \frac{u_{max}\, h_f}{\nu} \qquad (10)$$

where $u_{\max}$ was the maximum flow velocity at the fluid surface in the x direction and h_f the height of the fluid layer over the porous medium. Goharzadeh et al. [2005] argued that Re_f was based on a velocity in the free-fluid and hence, was not characteristic for the velocity in the entire domain. So, as it is customary in the literature, they introduced a *Reynolds number* Re_k based on the permeability of the porous medium and the Darcian velocity:

$$Re_k = \frac{u_{Darcy}\sqrt{k}}{\nu} \qquad (11)$$

Third, a *particle Reynolds number* was defined by using the grain size:

$$Re_p = \frac{u_{Darcy}\, d}{\nu} \qquad (12)$$

Finally, they considered a Reynolds number for the interfacial region:

$$Re_{int} = \frac{u_{int}\, d}{\nu} \qquad (13)$$

Another relevant parameter of a flow over a porous medium is the *Darcy number Da*:

$$Da = \frac{k}{\left(h_f + h_p\right)^2} \qquad (14)$$

Twelve numerical simulations were carried out using Multiphysics 3.5a™ to investigate the influence on the flow of (1) the permeability of the porous medium k, (2) the fluid-based Reynolds number Re_f and (3) the height of fluid layer above the porous medium h_f. They reproduced the experiments performed by Goharzadeh et al. [2005]. The first group of simulations, i.e. Run 1–5, was with Re_f=20.99, h_f=0.04 m and Da in the range from 8.13×10^{-8} to 2.43×10^{-6}. The second group, i.e. Run 6–9, was with Re_f from 6 to 17.04, h_f=0.04 m and Da=1.72×10^{-6}. The third group, i.e. Run 10–12, was with Re_f around 20.96, h_f from 0.02 to 0.05 m and Da=1.72×10^{-6}. Table 2 lists all the operative conditions, where all of the Reynolds numbers defined for the porous medium are much below 1.

Boundary conditions were assigned at the inlet, the outlet and at the walls of the domain:

- to obtain the parabolic velocity profile, the boundary condition at the inlet was $u_{in}=(6\cdot u_{avg}\cdot s\cdot(1-s)$, where u_{avg} is the average velocity and s is a boundary parameterization variable that runs from *0* to *1* along the boundary;

- at the outlet, a *zero pressure* type condition was assigned**;**
- at the wall above the free fluid, a *symmetry* type condition was assigned;
- at the walls besides and below the porous medium, a *no-slip* type condition was assigned;
- the fluid-porous interface was treated as an internal boundary and a *continuity* type condition was assigned.

Table 2. Key parameters of the numerical simulations

Run	k - m²	ε	u_{in} – *m/s*	*Da*	Re_f	Re_k	Re_{int}
1	5.2×10^{-10}	0.43	0.0150	8.13E-08	20.99	7.75E-09	6.66E-04
2	3.9×10^{-9}	0.41	0.0150	6.09E-07	20.99	1.58E-07	3.61E-03
3	5.2×10^{-9}	0.38	0.0150	8.13E-07	20.99	2.42E-07	2.99E-03
4	1.1×10^{-8}	0.41	0.0150	1.72E-06	20.99	7.47E-07	8.22E-03
5	1.3×10^{-8}	0.41	0.0150	2.03E-06	20.99	9.59E-07	1.24E-02
6	1.1×10^{-8}	0.41	0.0043	1.72E-06	6.00	2.15E-07	2.36E-03
7	1.1×10^{-8}	0.41	0.0072	1.72E-06	10.07	3.60E-07	3.96E-03
8	1.1×10^{-8}	0.41	0.0100	1.72E-06	14.00	5.00E-07	5.50E-03
9	1.1×10^{-8}	0.41	0.0122	1.72E-06	17.04	6.10E-07	6.70E-03
10	1.1×10^{-8}	0.41	0.0305	1.72E-06	20.99	6.00E-06	3.31E-02
11	1.1×10^{-8}	0.41	0.0201	1.72E-06	20.97	1.78E-06	1.47E-02
12	1.1×10^{-8}	0.41	0.0121	1.72E-06	21.06	3.89E-07	5.33E-03

Different mesh characteristics were tested. After that, the mesh generation process was made assuming, among the others, as *element growth rate* and *resolution of narrow regions* 1.3 and 1.00, respectively. The *element growth rate* determines the maximum rate at which the element size can grow from a region with small elements to a region with larger elements. The value must be greater or equal to 1. In the *resolution of narrow regions* field the number of layer of elements created in narrow regions is controlled. Finally, different values for the maximum element size were selected for the free fluid, the porous medium and the fluid-porous interface. Maximum elements sizes were 0.002, 0.005 and 0.00025 m for the free fluid, the porous medium and the fluid-porous interface, respectively. Overall, the used mesh had 48472 elements, with a minimum *element quality* of 0.672 (Fig.4). This parameter is related to the element aspect ratio, which means that anisotropic elements can get a low quality measure even though the element shape is reasonable. It is a scalar from 0 to 1. Mesh quality visualization demonstrated a uniform quality of the elements of the mesh.

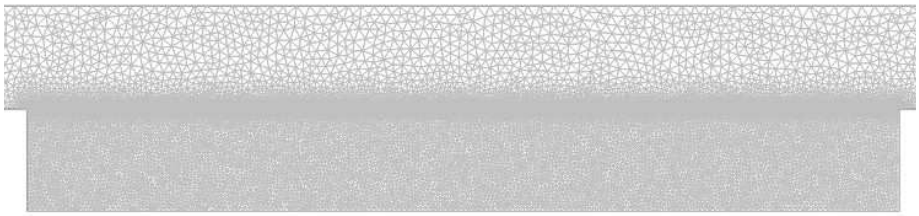

Figure 4. The generated mesh.

About the solver settings, stationary segregated solver with non-linear system solver was used, where the relative tolerance and the maximum number of segregated iterations were set to $1.0\cdot10^{-3}$ and 100, respectively. The segregated solver allows to split the solution steps into substeps. These are defined by grouping solution components together. This procedure can save both memory and assembly time.

4. NUMERICAL RESULTS. DISCUSSION

Numerical simulations provided velocity field and pressure values throughout the flow domain. The analysis of results was first focused to compare numerical velocity profiles with the experimental data. Fig.5 compares the *u* vertical profiles for Run 5. Fig.5a presents the profile in the entire domain, while Fig.5b is zoomed inside the porous region. Numerical

values tended to underestimated u values both in the free-fluid region and in the transition layer, whereas there is a reasonable agreement inside the porous medium.

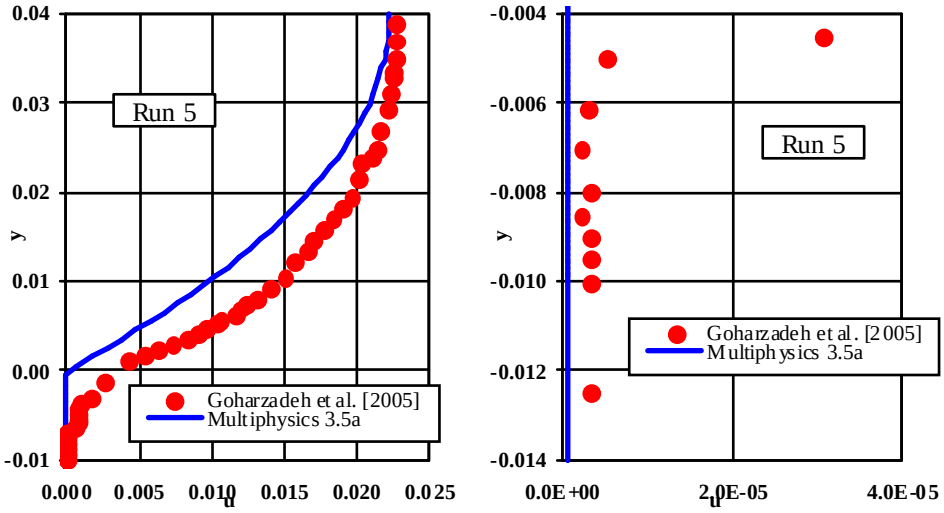

Figs. 5a/5b. Vertical *u* profiles. Overall plot (left), zoom inside the porous medium (right).

Second, numerical values of the thickness of the Brinkman layer δ_{Brink} were compares with the available experimental data. This thickness was obtained from the simulated velocity profile using the boundary layer thickness definition already applied by Goharzadeh et al. [2005]. Thus δ_{Brink} was defined as the distance below the fluid-porous interface at which the velocity first approaches to within 1% of the Darcy velocity u_D:

$$u = 1.01\, u_{Darcy}\Big|_{y=-\delta_{Brink}} \qquad (15)$$

Table 3 lists these values for Run 1–5. Comparison confirmed that numerical results were in the order of magnitude of the experimental data but underestimated the depth of the transition region.

Table 3. Numerical and experimental data of the thickness of the Brinkman layer

	δ_{Brink} – m	
Run	Multiphysics 3.5a	Goharzadeh et al. [2005]
1	0.0008	0.0024
2	0.0010	0.0036
3	0.0013	0.0023
4	0.0016	0.0043
5	0.0021	0.0060

Third, following what already carried out by Goharzadeh et al. [2005] using their experimental data, the analysis of the numerical results was addressed to investigate the influence of the permeability of the porous medium *k*, the fluid-based Reynolds number Re_f and the height of fluid layer above the porous medium h_f on the flow characteristics.

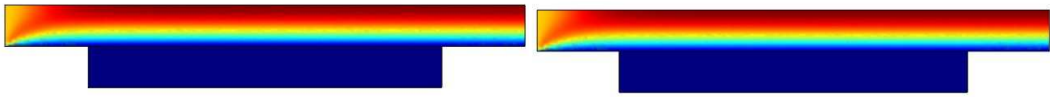

Figs. 6a/6b. Flow field. Run 1(left), Run 5 (right).

Run 1–5 provided information about the influence of the permeability. Fig.6 compares the flow field for the lowest and the largest permeability, i.e. Run 1 and Run 5. Larger

velocities are in red and low velocities in blue. Due to the increased permeability of the porous medium, the horizontal velocity component at the fluid-porous interface u_{int} increased from 8.37×10^{-6} m/s for Run 1 to 6.92×10^{-5} m/s for Run 5. Also, the thickness of the Brinkman layer δ_{Brink} increased with the increasing permeability from 0.0008 m to 0.0021 m from. This trend was consistent with that observed by Goharzadeh et al. in their experiments [2005].

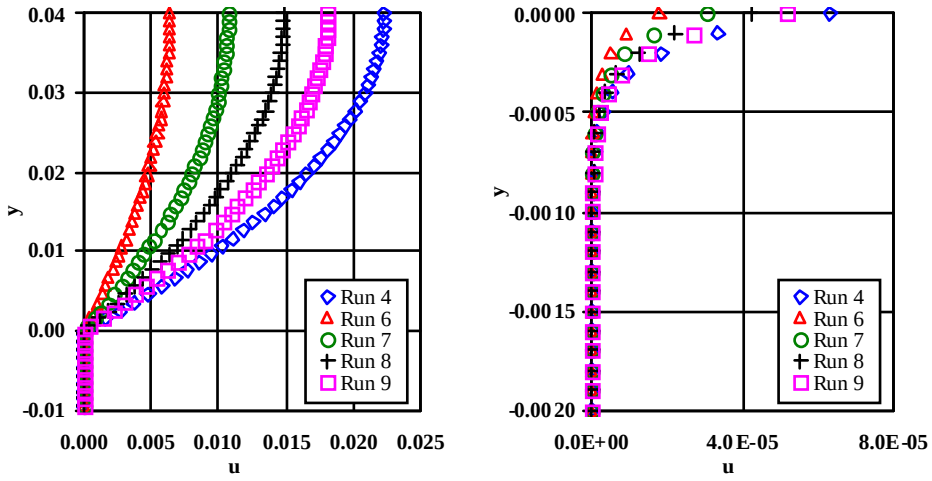

Figs. 7a/7b. Vertical *u* profiles. Overall plot (left), zoom at the interfacial region (right).

To study the response of the flow field to the fluid-based Reynolds number Re_f five numerical simulations can be considered, namely Run 4 and those from the second group of simulations, i.e. Run 6–9. Fig.7 shows the vertical profiles of the *x*-component *u* for these simulations. It can be noted that slopes of the velocity profiles depended on Re_f and they increased with the increasing Re_f both in the free-fluid and in the interfacial region. Furthermore, the thickness of the transition layer was not significantly changed. This results were consistent with previous literature findings (Choi and Waller, [1997]; Goharzadeh et al., [2005].

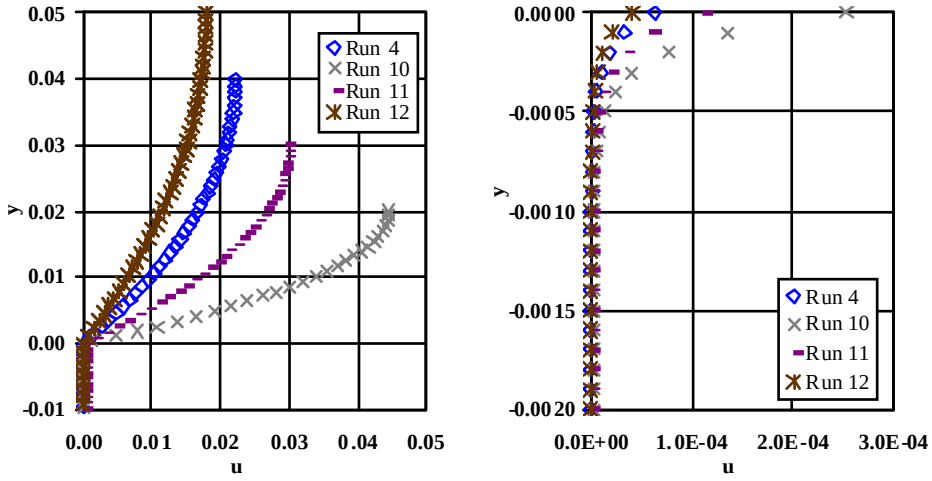

Figs. 8a/8b. Vertical *u* profiles. Overall plot (left), zoom at the interfacial region (right).

Four numerical simulations, namely Run 4 and Run 10–12, were used to investigate the

effect of fluid height h_f on the flow characteristics. Fig.8 reports the vertical profiles of u for these simulations. The slope of the u profiles increased with the decreasing h_f both in the free-fluid and in the interfacial region. The same trend was observed for u_{int}, whereas a clear trend for δ_{Brink} was missing. Again, these results were consistent with the experimental observations by Goharzadeh et al. [2005].

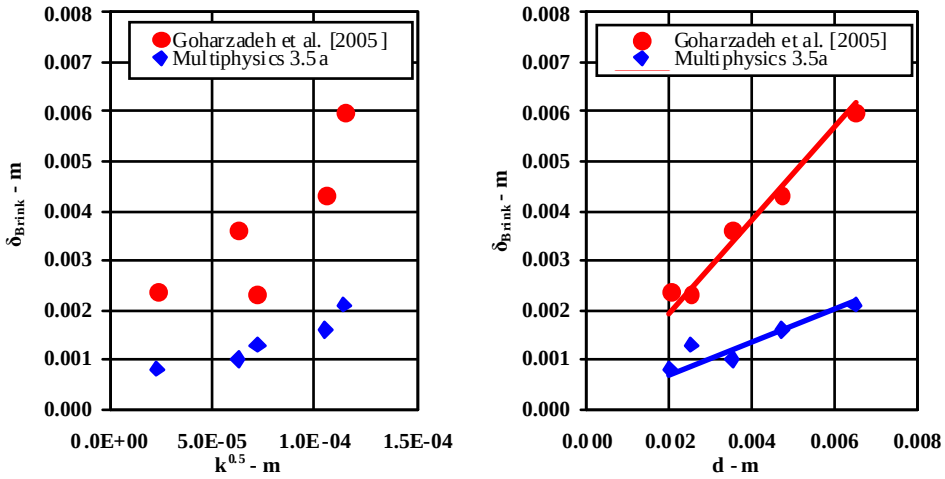

Figs. 9a/9b. Thickness of the Brinkman layer vs permeability (left), grain size (right).

Finally, both the simulated and the experimental thicknesses of the Brinkman layer were plotted against the square root of the permeability and the grain size. After all, numerical results confirmed the experimental finding that the length scale of the transition layer was in the order of grain diameter and much larger than the square root of permeability.

5. CONCLUSION.

The flow of a fluid over a permeable surface is a frequent case in the field of environmental hydraulics. It may be studied using the Brinkman equation, which describes the flow in porous media where momentum transport by shear stresses in the fluids is of importance. The paper presented the results of a numerical study of the flow in a free fluid-porous medium domain. Numerical results pointed out the strong effect of permeability on the flow characteristics and on the thickness of the layer inside the porous medium affected by the free-fluid flow. Also, the Reynolds number and the fluid height over the fluid-porous interface were found to affect the gradient of the horizontal velocity component at the interfacial region while the length scale of the transition layer remained approximately unchanged. These results were consistent with literature experimental finding although numerical results underestimated the thickness of the transition layer. Finally, they confirmed that this layer may be scaled with the grain size of the porous medium rather that with the square root of the permeability.

REFERENCES

Beavers, G.S., and Joseph, D.D., “Boundary conditions at a naturally permeable wall.”, *J. Fluid Mech.*, 30, 197–207, 1967.

Brinkman, H.C., “A calculation of the viscous force exerted by a flowing fluid on a dense swarm of particles.”, *Appl. Scient. Res.*, A1, pp.27–34, 1947.

Chan, H.C., Huang, W.C., Leu, J.M., and Lai, C.J., “Macroscopic modeling of turbulent flow over a porous medium.”, *International Journal of Heat and Fluid Flow*, 28, pp.1157–1166, 2007.

Choi, C.Y., and Waller, P. M., “Momentum transport mechanism for water flow over porous media.”, *Journal of Environmental Engineering, ASCE*, 123, 8, pp.792–799, 1997.

Darcy, H., “Les fontaines publiques de la ville de Dijon.”, Victor Dalmont, Paris, 1856.

Higashino M., Stefan H.G. and Gantzer C.J., "Periodic diffusional mass transfer near sediment/water interface: Theory.", *Journal of Environmental Engineering, ASCE,* 129, 5, pp.447–455, 2003.

Higashino, M., and Stefan, H.G., "Near-bed turbulence models: Significance for diffusional mass transfer at the sediment/water interface.", *Journal of Hydraulic Research, IAHR*, 46, 3, pp.291–300, 2008.

Huettel, M., Røy, H., Precht, E., and Ehrenhauss, S., "Hydrodynamical impact on biogeochemical processes in aquatic sediments.", *Hydrobiologia*, 494, 3, pp.231–236, 2003.

Goharzadeh, A., Khalili, A., and Jørgensen, B.B., "Transition layer thickness at a fluid-porous interface.", *Physics of Fluids*, 17, 057102, 2005.

Gualtieri, C., "Interaction between hydrodynamics and mass-transfer at the sediment-water interface.", *Proceedings of the iEMSs Second Biennial Meeting: International Congress on Environmental Modelling and Software* (*iEMSs 2004*), Osnabrück (Germany), June 14/17, 2004.

Gualtieri, C., "Discussion on M.Higashino, H.G.Stefan and C.J.Gantzer: Periodic diffusional mass transfer near sediment/water interface: Theory. J. Env.Eng., ASCE, vol.129, n.5, May 2003. pp.447–455.", *Journal of Environmental Engineering, ASCE,* 131, 1, pp.171–172, 2005.

Gupte, S. K., and Advani, S.G., "Flow near the permeable boundary of a porous medium: An experimental investigation using LDA.", *Experiments in Fluids*, 22, pp.408–411, 1997.

James, D.F., and A.M., Davis, "Flow at the interface of a model fibrous porous medium.", *J. Fluid Mechanics*, 426, pp.47–72, 2001.

Lorke, A., Müller, B., Maerki, M., and Wüest, A., "Breathing sediments: The control of diffusive transport across the sediment-water interface by periodic boundary-layer turbulence.", *Limnology and Oceanography*, vol.48, n.6, pp.2077–2085, 2003.

McNair, J. N., Newbold, J. D., and Hart, D. D., "Turbulent transport of suspended particles and dispersing benthic organisms: How long to hit bottom ?.", *J. Theor. Biol.*, 188, 1, pp.29–52, 1997.

Multiphysics 3.5a, "User's Guide." ComSol AB, Sweden, 2009.

Ochoa-Tapia, A.J., and S., Whitaker, "Momentum transfer at the boundary between a porous medium and a homogeneous fluid. I: Theoretical development.", *Int. J. Heat Mass Transfer*, 38, 14, pp.2635–2646, 1995.

Packman, A. I., Salehin, M., and Zaramella, M., "Hyporheic exchange with gravel beds: Basic hydrodynamic interactions and bedform-induced advective flows.", *J. Hydraul. Eng.*, 130, 7, pp.647–656, 2004.

Pokrajac, D., and Manes, C., "Interface between turbulent flows above and within rough porous walls.", *Acta Geophysica*, 56, 3, pp.824–844, 2008.

Prinos, P., Sofialidis, D., and Keramaris, E., "Turbulent flow over and within a porous bed.", *Journal of Hydraulic Engineering, ASCE* 129, 9, pp.720–733, 2003.

Steinberger, N., and Hondzo, M., "Diffusional mass transfer at sediment-water interface.", *J.Env.Eng.Div. ASCE*, vol.125, n.2, pp.192–200, 1999.

Tan, H., and Pillai, K.M., "Finite element implementation of stress-jump and stress-continuity conditions at porous-medium, clear-fluid interface.", *Computers & Fluids*, 38, pp.1118–1131, 2009.

Vafai, K., and Kim, S.J., "Fluid mechanics of the interface region between a porous medium and a fluid layer: an exact solution.", *Int. J. Heat Fluid Flow*, 11, pp.254–256, 1990.